International Communications in Heat and Mass Transfer 148 (2023) 107057

Contents lists available at ScienceDirect

International Communications in Heat and Mass Transfer

journal homepage: www.elsevier.com/locate/ichmt

An experimental investigation on the influence of condenser bypass area for the transient and steady-state heat-transfer performance of heat pipes

Cheong Hoon Kwon [a], Hyuk Su Kwon [b], Eui Guk Jung [b,*]

[a] Department of Energy Resources and Chemical Engineering, Kangwon National University, Kangwon-do 25913, Republic of Korea
[b] School of Mechanical System Engineering, Kangwon National University, Kangwon-do 25913, Republic of Korea

ARTICLE INFO

Keywords:
Thermal resistance
Bypass mass flow rate
Temperature overshoot
Heat pipe
Liquid-bypass line

ABSTRACT

Fundamentally, an effective method for improving the performance of transient and steady-state heat transfer is reducing the flow resistance at the phase-change interface based on the counter flow of vapor and liquid within a typical heat pipe. The flow resistance at such an interface is proportional to the volume flow rates of liquid and vapor. Therefore, the flow resistance at the interface can be reduced by limiting the mass flow rate of vapor or liquid. In this study, experiments were performed on a liquid bypass to improve the steady-state thermal performance of heat pipes. A separate bypass tube allowed some liquid to be subcooled in the condenser to bypass the evaporator without passing through the heat pipe. Three liquid-bypass ports were designed and fabricated in a condenser to experimentally investigate the influence of the bypass port area on the thermal performance of the heat pipe under steady-state operation. An on/off valve was attached to each bypass tube port in the condenser to control the bypass flow rate. The results showed that the thermal resistance, an evaluation index of the performance of steady-state heat transfer, generally decreased with an increase in the bypass port area of the condenser. The thermal resistance of a heat pipe with a horizontal tilt angle and one at an inclination angle of 50° decreased by up to 25.5% and 51.6%, respectively.

1. Introduction

Thermal energy management is essential for operating mechanical systems, electronics, and electrical components. For example, high-temperature environments because of heat generated by electrical resistance may seriously threaten the normal operation of highly integrated electronic equipment. A typical heat pipe is an effective thermal management device that can transport thermal energy over long distances and requires no external power. A typical heat pipe is a two-phase thermal-control device with highly effective thermal conductivity; circulation from liquid to vapor or vapor to liquid occurs between the evaporator and the condenser. Heat exchangers using typical heat pipes can be delineated as smaller than conventional heat exchangers when dealing with high heat fluxes because of their high heat-transfer capability [1]. The application of heat-pipe technology has been extended to many fields to enhance the heat-transfer performance of heat-pipe-based heat sinks in micro-level electronic engineering. Considering the confined package environment of highly integrated electronic products, typical heat pipes have attracted attention as thermal management devices for electronic equipment because no additional external power is required, the working fluid and electronic circuit can be completely electrically insulated, and the heat generation and dissipation parts can be separated. Typical heat pipes have also been widely applied as cooling devices in other industries, such as traditional heating, ventilation, air conditioning (HVAC) systems, temperature control systems for spacecraft, human bodies [2], and various nuclear reactor technologies. In recent years, research has been conducted to apply typical heat pipes to solar energy and thermal management systems for electric vehicle batteries [3]. Previous efforts to develop high-performance heat pipes have extended their applications to the heat-transfer control of electronic components in space vehicles, including satellites and spacecraft, and mechanical systems with various ground heat sources [4–6].

A typical heat pipe is an independent cylindrical structure that achieves a very high heat transfer using a two-phase capillary flow, as shown in Fig. 1. The typical heat pipe operates under a two-phase flow regime, that is, a device with a vaporization–condensation procedure to transfer thermal energy. The vapor that absorbs latent heat in the evaporator can travel a long distance to the condenser. In the condenser, the latent heat is released into the cold source, so the vapor condenses into a liquid, cools, and the returns to the evaporator. The driving force

* Corresponding author.
E-mail addresses: chkwon2@kangwon.ac.kr (C.H. Kwon), egjung@kangwon.ac.kr (E.G. Jung).

https://doi.org/10.1016/j.icheatmasstransfer.2023.107057

Available online 25 September 2023

Nomenclature

BOM	bypass line operation mode
BL	bypass line
BLFV	bypass line flow valve
NOM	normal operation mode
Q	thermal load (W)
T	temperature (°C)
$\overline{T}$	mean temperature (°C)
U	uncertainty
φ	inclination angle of the heat pipe (degree)
Φ	fill–charge ratio of working fluid

Subscripts

adia.	adiabatic
BL	bypass line
con.	condenser
cool. i	coolant inlet
cool. o	coolant outlet
eva.	evaporator
in	input
max.	maximum value
m	measurement

in heat-pipe operation is the vapor pressure difference between the evaporator and condenser and the capillary pressure generated by the curvature of the phase-change interface in the pores of the wick structure with a pressure difference between vapor and liquid. The condensed and cooled liquid in the condenser returns to the evaporator through the wick via capillary pressure. Therefore, previous studies on improving the heat transfer performance of typical heat pipes have mainly focused on supplying favorable capillary pressure by applying new design techniques for capillary structures [5–13] or the working fluid [14–17]. Li et al. [6] fabricated Ω-shaped and trapezoidal grooves in typical heat pipes and presented experimental results that compared their startup performance. They found that Ω-shaped grooves yielded a better startup performance owing to the favorable working fluid acceleration at an appropriate geometrical configuration. Zhao et al. [7] applied a composite wick that combined different screen mesh capillary structures to a typical heat pipe using sodium as a working fluid and compared its heat-transfer performance with a single screen mesh wick. They found that the thermal resistance was significantly lowered under the operation of a typical heat pipe with a composite wick. In an experiment on the thermal performance of flat micro heat pipes, Zhao et al. [8] obtained up to a 14% increase in thermal performance by applying sintered metal capillary structures with different particle sizes compared to those that used single sintered metals. Wong et al. [9] experimentally obtained an improved maximum heat-transfer performance by applying a composite wick that properly combined different mesh numbers for the screen capillary structure, which enabled a higher capillary pressure to be secured. Zhou et al. [10] introduced, tested, and verified the thermal performance of a woven wire wick with improved adhesion between the heat-pipe wall and the capillary wick due to its reinforced elasticity. Huang et al. [11] experimentally confirmed the characteristics of a single sintered wick with improved heat-transfer performance in the oxidation process under an appropriate temperature in an experiment on a very thin flat plate heat pipe. Huang et al. [12] introduced a new composite wick made of stainless-steel powder and fibers and verified its high performance through an experimental comparison of heat-transfer performance with existing powder or fiber wicks. Wong et al. [13] compared the heat-transfer performance between a mesh-grooved wick and a two-layer screen wick with a 200 mesh, and an increased capillary force was confirmed under the application of the mesh-grooved composite wick.

Some studies have improved the heat-transfer capacity of typical heat pipes by considering the working fluid. Henein and Abdel-Rehim [14] used a nanofluid as the working fluid. They obtained the best heat-transfer capacity for a hybrid nanofluid of magnesium oxide with multi-walled carbon nanotubes. Zhang et al. [15] studied the thermal response of magnetic fluid as the operating fluid in a flat heat pipe. The magnetic fluid yielded a more even heat flux in the condenser than in water. Ayel et al. [16] used three binary aqueous mixtures as the working fluid and experimentally compared their heat-transfer performance. The transient characteristics of these binary mixtures compared to those of pure water were presented in detail.

Studies have been conducted on improving heat transfer through structural changes and physical considerations inside heat pipes. In a typical heat-pipe operation, heat transfer is significantly limited owing to the flow resistance over the interface caused by the counter flow of vapor and liquid. A heat pipe with a loop shape, in which vapor and liquid are completely separated, has been developed to overcome this weakness. [17]. Wu et al. [18] fabricated a novel type of heat pipe suitable for cooling the spent fuel pool by completely separating the vapor and liquid tubes of the evaporator and condenser. Experimental results were provided on the cooling performance. Kang et al. developed numerical models for a pulsating heat pipe with a single loop. These models predicted significant improvements in the heat-transfer performance of the porous wicking layer [19] and separating walls [20] inside the flow channel. Kang et al. [21] also fabricated a flexible transport tube for the working fluid. In addition, a pulsating heat pipe was fabricated, and multiple heat sinks were applied, after which the heat-transfer performance of the system was determined through experimentation. In particular, applying a flexible transport tube for the working fluid can be very useful for effective thermal management in a limited space. The application of multiple heat sinks can be evaluated as a module-level thermal-control technology for various electronic components. Kang and Fan [22] fabricated and tested a loop-type thermal rectifier, which applied the principle of a heat pipe. In their study, a thermal rectification ratio of up to 4.18 was achieved for both a constant heat flux of forward heating using an open valve and reversed heating using a closed valve with thermal rectifiers and on/off valves attached to the vapor transport tube.

Heat pipes with separated vapor and liquid have significantly improved heat-transfer performance compared to typical heat pipes because the flow resistance produced by the counter flow between the vapor and liquid can be eliminated. In particular, the loop heat pipe has a strong advantage in space applications because it can operate normally under gravity unassisted, where the evaporator is above the condenser. However, a very high level of technology is required to design and manufacture heat pipes using these loop configurations. Notably, for a

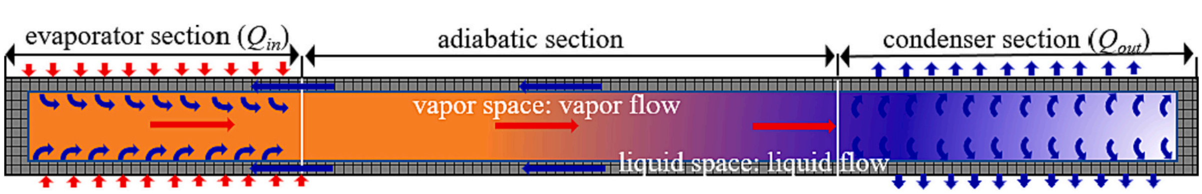

Fig. 1. Schematic of a typical heat pipe including the flow of the working fluid.

typical loop heat pipe to operate normally, a high level of sintering technology for a fine porous wick is required, and the manufacturing cost is high, so there is a limit to its application in the thermal control of electronic components for ground use.

However, studies were recently conducted to investigate the thermal performance enhancement associated with a pressure drop in the working fluid using physical considerations of the vapor and liquid, which have counter flows inside the typical heat pipe [23,24]. In these studies, bypass lines that connect the evaporator and condenser were devised so that some liquid inside the condenser could bypass the evaporator without passing through the heat pipe. In these studies, the maximum heat transfer [23] was improved by up to 35.5% as the working fluid acceleration was produced, owing to the reduction in the pressure drop inside the heat pipe under the application of the bypass line. In addition, the thermal resistance [24] under steady-state operation was reduced by up to 61%. Furthermore, the effect of the bypassed flow rate on the operating limit with an increase in the condenser area open to the bypass tube was investigated relatively recently by Cheong et al. [25]. They installed three bypass ports in the condenser and investigated the variation in maximum input thermal load according to the number of activated bypass ports. In their study, the maximum input thermal load increased with an increase in the number of activated bypass ports, and when all three bypass ports installed in the condenser were opened, the maximum thermal load increased by up to 45.8%. Additionally, literature [25] provided theoretical background showing that the maximum heat transfer rate can be increased by increasing the mass flow rate of the bypassed liquid. These experiments showed that reducing liquid mass flow in a typical heat-pipe space significantly improved heat-transfer performance. Heat pipes with bypass lines differ from those with loop types in that they partially separate vapor and liquid. Therefore, while maintaining the advantages of a loop-type heat pipe, a very simple and economical design is possible for manufacture.

Previous studies have investigated how liquid bypasses contribute to heat-transfer performance [23,24], with schematic outputs as shown in Fig. 2. In particular, the operating limit of the heat pipe is improved with an increase in the area of the condenser open to the bypass tube [25]. As shown in Fig. 3(b), the bypass line can partially separate the liquid from the heat-pipe space. The liquid can be bypassed when the bypass line is positioned below the heat pipe. However, the vapor can be bypassed above the bypass line heat pipe. Because the flow resistance of the working fluid in the inner space of the heat pipe can be further reduced as the flow rate of the bypassed liquid or vapor increases, a greater heat-transfer performance can be expected by increasing the acceleration performance of the working fluid. Therefore, a more effective bypass tube design should be considered to allow as much liquid as possible to be bypassed. In a previous study [25], the maximum input thermal load of the heat pipe was investigated for change in mass flow rate bypassed liquid in the heat pipe. However, transient and steady-state heat transfer performance with increases in the flow rate of the bypassed liquid has not been experimentally reported.

This study was conducted as an extension of the previous study [25], and the purpose was to experimentally obtain the effect of an increase in the mass flow rate of the bypassed liquid on the transient and steady-state thermal performance of the heat pipe. The effect of increasing the opening area of the condenser to the bypass tube, which was not covered in previous studies [23–25], on the transient and steady-state heat-transfer performance of the heat pipe was experimentally presented. As shown in Figs. 2 and 3(b), three liquid-bypass ports were attached to the condenser as in the previous study [25] to investigate the influence of the liquid flow rate bypassed from the condenser to the evaporator on the heat-transfer performance of the heat pipe. The heat-pipe system was designed to manually control the flow rate of the bypassed liquid according to the number of bypass ports activated. Because the typical heat pipe is operated under a saturation condition with a two-phase flow, a method for measuring the pressure and mass flow rate using instrumentation has not been previously developed. Therefore, it was assumed that the bypassed mass flow rate increased when more bypass ports were activated. Experiments were conducted on the heat-transfer trend under four operating modes according to the number of activated bypass ports. The activated bypass port area is defined as the area of the condenser open to the bypass tube.

For convenience, three areas equal to the inner diameter of the bypass tube, located at the start, middle, and end of the condenser, were opened to the bypass tube at equal intervals. As shown in Fig. 2, the bypass mass flow rate can be controlled by activating ports individually using the bypass valve. The experimental results on the transition and steady-state heat-transfer performance changes according to the number of activated bypass ports are presented. The mass flow rate of the liquid to be bypassed is assumed to be strongly dependent on the area or location of the bypass port attached to the condenser. However, an analytical model capable of effectively designing the bypass flow path of the condensation unit is not yet known, and an appropriate model capable of predicting the bypassed liquid mass flow rate has not been previously developed. Therefore, this study is limited to an experimental approach, and a theoretical approach for a heat pipe with a bypass line is beyond the scope of this study.

2. Experimental setup and procedure

The experimental setup of this study and the geometric dimensions of the heat pipe with the bypass tube are the same as those in the literature [25]. As shown in Fig. 3, bypass tubes with three bypass ports (Fig. 3(b)) are attached to the condenser of a typical heat pipe (Fig. 3(a)). Bypass ports were attached to the start, middle, and end of the condenser at equal intervals. A flowrate on/off valve was attached to each port. The valves were sequentially activated from the start of the condenser to regulate the mass flow rate of the liquid bypass. The highest mass flow rate was bypassed to the evaporator without passing through the internal space of the heat pipe when all three bypass valves were opened.

The basic geometric configuration of the groove machined on the inner wall of the heat pipe to supply capillary pressure is shown in Fig. 4, where the trapezoidal groove supplies the driving force required for the circulation of the working fluid. Each groove had a height of 2 mm height, 0.7 mm base length, and 0.93 mm tip length. The heat pipe and bypass tubes were made of aluminum. As presented in Fig. 4, the outer and inner diameters were 15.88 and 13.88 mm, respectively. *A*1-mm-thick aluminum tube was used. The entire length of the heat pipe was 750 mm, the lengths of the evaporator and condenser were 200 mm, and

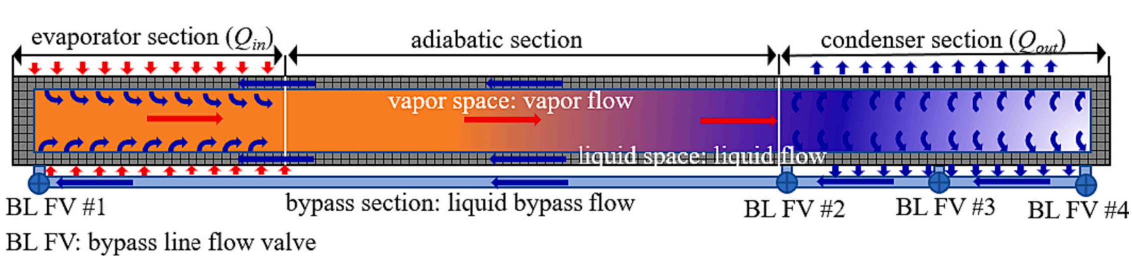

Fig. 2. Physical operating principle of a heat pipe with a bypass line with three bypass ports in the condenser; four bypass line flow valves (BLFVs) are present.

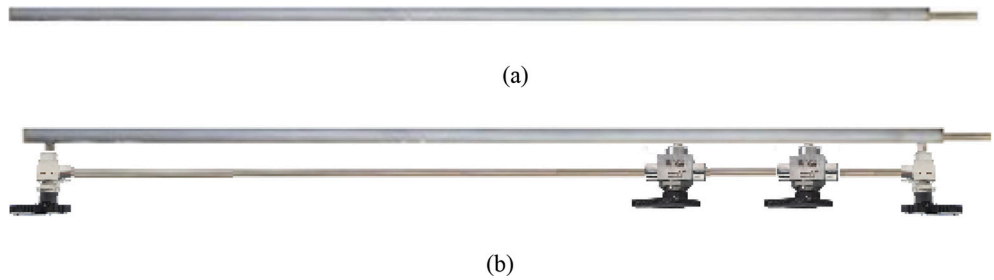

Fig. 3. Photographs of (a) a typical heat pipe and (b) a heat pipe with a bypass line with three bypass ports in the condenser, as considered in this study [25].

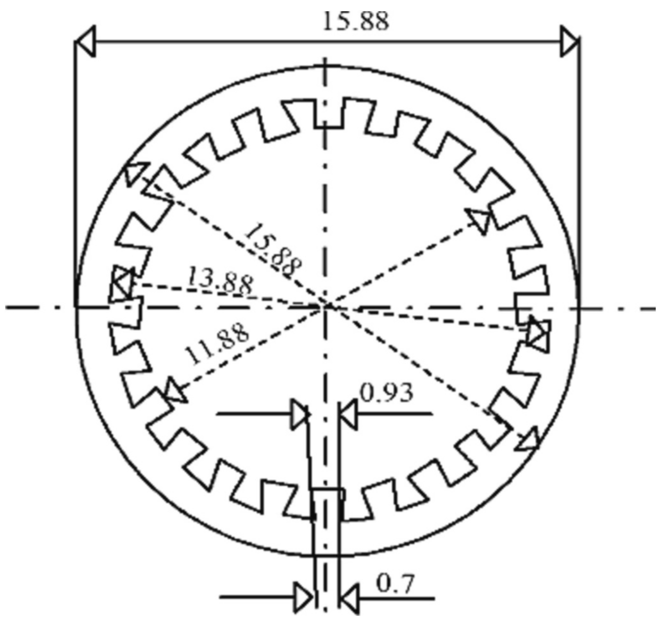

Fig. 4. Cross-sectional diagram of the grooved heat pipe.

the remaining 350 mm was designed as an adiabatic section. The bypass line had a 6.35 mm outer diameter, and the length of the straight portion was 747 mm. A bypass port was installed at the start of the evaporator. Three bypass ports attached to the condenser were installed at the start (550 mm), middle (648 mm), and end (747 mm) of the condenser. A bypass line flow valve (BLFV) was installed at each bypass port to regulate the liquid-bypass flow rate. As shown in Figs. 4 and 5, 3-way valves (BLFV #2 and #3) made of stainless steel were attached to two ports to control the liquid-bypass mass flow rate. Two 2-way valves (BLFV #1 and #4) were attached to the start of the evaporator and end of the condenser to secure the bypass flow path.

A fill tube was attached to the condenser to charge the working fluid. The fill–charge ratio of the operating fluid was evaluated based on the NOM. If the fill–charge ratio is excessive, the liquid pool generated at the start of the evaporator can hinder the heat transfer to the condenser during bubble formation caused by nucleate boiling [26,27]. However, if the amount of charging is insufficient, the Q_{in} that the typical heat pipe can operate may decrease. Therefore, the operating fluid's charging amount must be correctly determined through experimentation. Moreover, the fill–charge ratio of the working fluid was estimated based on the void volume of all grooves machined in the heat pipe.

As depicted in Figs. 2 and 3, the positions and number of bypass ports installed in the condenser significantly affected the liquid-bypass mass flow rate. Therefore, the number of activated bypass ports placed in the condenser was an important variable in this experiment. Generally, the working fluid is selected by considering its compatibility with the operating temperature range of the wall material. This study used 99%

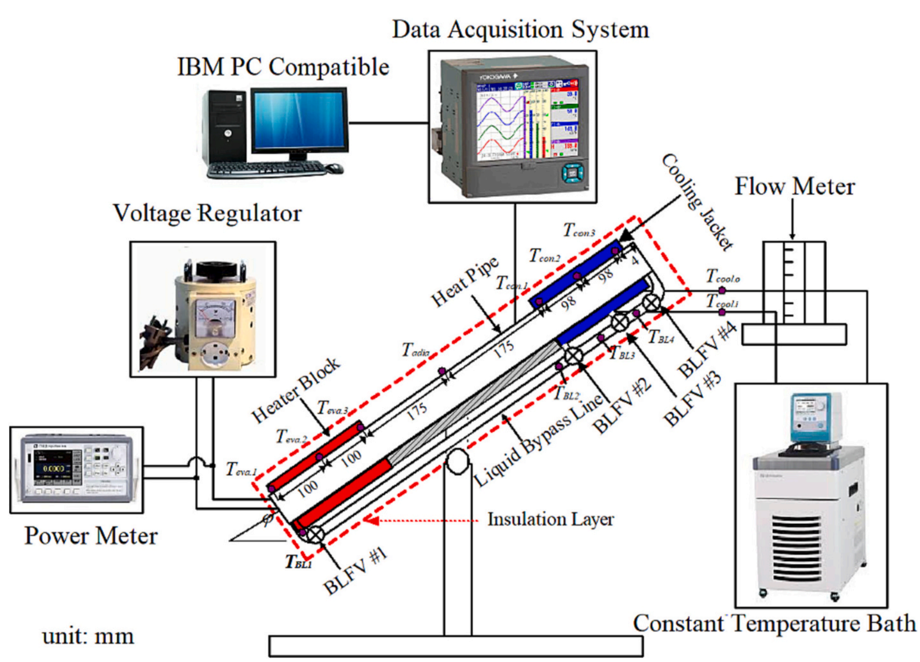

Fig. 5. Experimental setup of the proposed heat-pipe system, including the locations of the thermocouples.

pure acetone, with excellent compatibility with aluminum, as the working fluid. The inner space of the heat pipe was filled with a working fluid under a pressure of 1.1 × 10^{-5} Torr or less using a high vacuum pump. As shown in Fig. 5, the cooling jacket, where the coolant flows, was designed to cover the condenser. Pure water was used as the coolant, and the temperature of the coolant was kept constant using an isothermal bath. The isothermal bath had a maximum isothermal capacity of 1 kW based on 3 °C, and the coolant temperature was kept constant at 3 °C. Throughout the experiment, the volume flow rate ($\dot{V}$) of the coolant was detected using a rotameter with an uncertainty of 4% of the maximum full scale (4 L/min) and was constantly controlled to 3 L/min.

The input thermal load (Q_{in}) was supplied to the heat pipe by inserting four 1-kW electrical-resistance cartridge-type heaters into the aluminum heater block that covered the entire evaporator. The capacity of the heater was selected such that a sufficient thermal load could be supplied, considering that the maximum thermal load for normal operation of the heat pipe strongly depends on the orientation of the heat pipe, working fluid, and cooling conditions. A constant input thermal load was regulated to a constant value by a voltage regulator (wattmeter) and monitored employing a power meter with an uncertainty of 0.5% of full scale. The temperature was measured at seven selected positions along the axial direction of the heat pipe, as shown in Fig. 5. The thermocouples employed in the experiment were K-type, with an AWG number of 30 and a wire diameter of 0.25 mm. The tip of each thermocouple was firmly bonded to the external wall of the heat pipe using welding and an OMEGA bond (OB-200). Three thermocouples were employed to monitor the temperature of the outer wall of the evaporator: $T_{eva.1}$, $T_{eva.2}$, and $T_{eva.3}$, which were bonded to the start, middle, and end of the evaporator, respectively, with equal spacing (Fig. 5). A thermocouple was attached at the midpoint of the adiabatic section to measure the representative temperature of that section: T_{adia}. In a typical heat-pipe experiment, the temperature ($T_{adia.}$) of the adiabatic section can be defined as the operating, liquid, and vapor temperatures, assuming that the liquid and vapor are in a local equilibrium state. Three thermocouples were used to monitor the temperature of the external wall of the condenser: $T_{con.1}$, $T_{con.2}$, and $T_{con.3}$ were attached to the condenser's start, middle, and end with equal spacing, respectively.

The liquid-bypass flow was detected using four thermocouples attached to the bypass lines (T_{BL1}, T_{BL2}, T_{BL3}, and T_{BL4}). The thermocouples had the same specifications as those bonded to the external walls of the heat pipe. Their attachment positions were close to the outlet of each bypass valve so that they could monitor the bypass flow passing through the valve. The temperatures at the entrance and exit of the coolant ($T_{cool.i}$ and $T_{cool.o}$) were measured using thermocouples with a 3 mm probe inserted into both the entrance and exit of the cooling jacket to investigate the heat-transfer rate from the condenser to the coolant. All thermocouples were calibrated by a standard analog thermometer within a temperature error of 0.1 °C in the 3–100 °C range. Accordingly, all the temperature data measured using the thermocouples were corrected based on this analog thermometer. The temperature data were sensed and stored every second via a data acquisition (DAQ) system and stored using software, as shown in Fig. 5. The uncertainties of the instruments used in the heat-pipe system are listed in Table 1. These uncertainties were obtained from instrument manufacturers. The uncertainty of the entire experimental setup was evaluated using the equation presented in [25,28]. The system uncertainty for the experimental setup with N instruments is expressed as Eq. (1) using the square root of the sum of squares (SRSS).

$$U_m = \sqrt{U_1^2 + U_2^2 + U_3^2 + \dots + U_N^2} \tag{1}$$

When the uncertainty for each of the five instruments presented in Table 1 is applied to Eq. (1), the uncertainty of the experimental device is determined to be 4%. All elements of the heat-pipe system were washed using an ultrasonic cleaner charged with acetone to minimize the production of non-condensable gas inside the heat pipe. All experiments were performed in a laboratory environment at a constant temperature, and the entire test set was isolated using ceramic wool to hinder heat exchange with the external environment. As shown in Fig. 5, thermal contact between the bypass tube and the ambient environment is prevented because the heat pipe firmly insulates the bypass tube. However, the input thermal energy may be conducted through the wall of the bypass tube attached to the start of the evaporator via thermal conduction. In addition, the bypass tube located in the condenser can be cooled by heat conduction.

As outlined in Section 1, the main purpose of this experimental work was to measure the thermal performance of the heat pipe for different numbers of activated bypass ports in the condenser under a steady state. To this end, the on/off bypass valves attached to the condenser (Fig. 5) were the major experimental variables. As shown in Figs. 2 and 5, the control valve at the start of the evaporator (BLFV#1) and one of the three bypass valves attached to the condenser must be opened to activate the bypass line. The bypass operation mode (BOM) is defined as a scenario in which the bypass port is activated for liquid bypass. The bypass mass flow rate can be controlled using three bypass valves at the start, middle, and end of the condenser (BLFV #2, #3, and #4, respectively). Each bypass port was activated by opening the corresponding bypass valve attached to each position of the condenser. Table 2 summarizes the four operation modes investigated in this study: NOM, in which all bypass valves are closed; BOM I, in which the valves located at the start of the evaporator and condenser are opened; BOM II, in which the valves located at the start of the evaporator and the start and middle of the condenser are opened; and BOM III, in which all bypass valves attached to the heat pipe are opened. These four operation modes were investigated in all the experiments. We estimated that the bypass mass flow rate will increase as the bypass valves in the condenser from BLFV #2 to #4 are sequentially opened. The heat-transfer performance for these operating procedures was compared and analyzed in terms of R_{th} based on the measured temperature data under steady-state operation.

3. Results and discussion

A sequence of experiments was performed to measure the transient and steady-state thermal performances according to the variation in the bypass flow rate. The orientation of the heat pipe and input thermal load were designated as the main experimental variables. The maximum orientation of the heat pipe was limited to 50°, considering the temperature control capacity of the constant-temperature bath.

Fig. 6 shows the R_{th} of the NOM heat pipe according to the fill charge ratio (Φ) of the working fluid as a function of the Q_{in}. The heat pipe was horizontal, and the coolant temperature was 3 °C. The volume for the

Table 1
Uncertainties of the instruments used in experiments [25].

Independent variable	Error (gauge)	Uncertainty
Thermocouple (OMEGA, K-type, 30 AWG)	0.5 °C	0.00175
Thermal load (ITECH, IT9121)	0.5%	0.005
Isothermal bath (DAIHAN, CL-30)	0.1 °C	0.0004
Data acquisition system (YOKOGAWA, GP10)	0.01%	0.0001
Flow meter (Dwyer, RMA - 2)	0.5 cc	0.04

Table 2
Operation modes considered in experiments [25].

Operation mode	BLFV #1	BLFV #2	BLFV #3	BLFV #4
	ON/OFF	ON/OFF	ON/OFF	ON/OFF
NOM	OFF	OFF	OFF	OFF
BOM I	ON	ON	OFF	OFF
BOM II	ON	ON	ON	OFF
BOM III	ON	ON	ON	ON

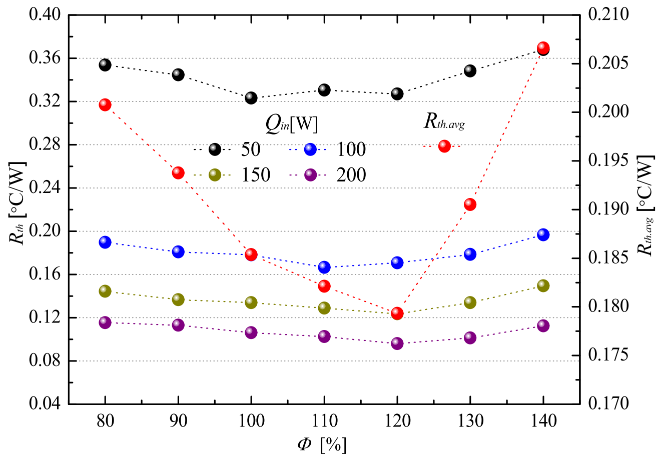

Fig. 6. Comparison of R_{th} according to Φ as a function of Q_{in} for a heat pipe with $\varphi = 0°$.

working fluid with $\Phi = 100\%$ corresponds to the total void volume of the groove. In particular, the thermal resistance, $R_{th.avg}\left[= \left(R_{th}|_{Q_{in}=50\ W} + R_{th}|_{Q_{in}=100\ W} + R_{th}|_{Q_{in}=150\ W} + R_{th}|_{Q_{in}=200\ W}\right)\Big/4\right]$, indicated on the axis on the right side of Fig. 6 is the average value of the thermal resistance measured at all input thermal loads (50 W, 100 W, 150 W, and 200 W). The fill–charge ratio (Φ) increased by 10%, from 80% to 140%. For all Q_{in}, the highest thermal resistance was measured at a fill–charge ratio of 140%, resulting in poor heat-transfer performance. As shown in Fig. 6, when Φ increased to 120%, the average thermal resistance was measured to be the lowest. From the results in Fig. 6, Φ of the working fluid in all experiments corresponded to 120% of the void volume of the grooves, and the amount of charging of the working fluid was 17.6 mL.

In a previous study [25], an experiment was conducted to compare the thermal performance of a typical heat pipe (Fig. 3(a)) and a heat pipe with a bypass tube operating under the normal operation mode (NOM), in which all flow rate control valves were closed. The presence of the bypass line resulted in a difference in the thermal performance between the NOM and typical heat pipe. This difference is because the physical environment generates the flow resistance when the working fluid reaches the flow rate control valve inlets through the bypass ports, even when all bypass valves are closed under NOM conditions. Fundamental and basic experimental results to evaluate the reliability of the experimental device and heat pipe system of this study were provided in ref. [25].

The results of comparing the thermal resistances of the typical and NOM heat pipes situated horizontally are provided in ref. [25]. The thermal resistance was evaluated using Eq. (2) and is an important indicator in thermal performance evaluation.

$$R_{th} = (\overline{T}_{eva.} - \overline{T}_{con.})/Q_{in} \tag{2}$$

where $\overline{T}_{evap}$ and $\overline{T}_{cond}$ are the average temperatures on the outer walls of the evaporator and condenser, respectively. As presented in a previous study [25], the maximum error between typical and NOM heat pipes was measured to be up to 13% at an input thermal load of 50 W but was found to be less than 5% at other thermal loads.

The uncertainty in thermal resistance presented in Eq. (1) was reviewed with reference to [28] and is presented in Eq. (3).

$$U_{R_{th}} = \pm\left[\left(\frac{\overline{T}_{eva.}}{\overline{T}_{eva.} - \overline{T}_{con.}} \times U_{\overline{T}_{eva.}}\right)^2 + \left(\frac{\overline{T}_{con.}}{\overline{T}_{eva.}} \times U_{\overline{T}_{con.}}\right)^2 + U_{Q_{in}}\right]^{1/2} \tag{3}$$

As presented in the literature [25], the discrepancy in the thermal resistance uncertainty between the typical and NOM heat pipes is less than 4% overall, and the maximum difference is estimated at 3.6%. The uncertainty of the measured thermal resistance of the heat pipe with NOM was estimated to be less than 11% overall, and the maximum uncertainty was 10.1%.

The recovery energy (Q_{out}) released from the condenser to the coolant is defined by

$$Q_{out} = \left(\rho \dot{V} c\right)_{cool}(T_{cool.o} - T_{cool.i}) \tag{4}$$

where $\dot{V}$ is the volume flow rate of the coolant across the condenser. At horizontal configuration, based on the energy conservation between the Q_{out} released to the coolant through the heat pipe and Q_{in}, the heat loss to the surroundings was presented in [25]. From ref. [25], heat loss increased with an increase in input thermal load, and the minimum and maximum heat losses in the entire input thermal load range were found to be 5.1% and 7.9%, respectively. Heat loss was generally within 10% of the input thermal load.

Experimental studies were performed to investigate the heat-transfer performance of the heat pipe according to the number of activated bypass ports in the condenser under transient and steady-state operations. The experimental variables are the orientation of the heat pipe, Q_{in}, and heat-pipe operation modes presented in Table 2. The coolant temperature was constant at 3 °C, and all other experimental parameters were fixed. Because of the limited cooling capacity of the isothermal bath used in the experiment, the inclination angle of the heat pipe, φ, was constrained to a maximum of 50°. As depicted in Fig. 3, the heat pipe with NOM was geometrically identical to a typical heat pipe when bypass line components were excluded. The thermal performances of the NOM and typical heat pipes were tested in a preliminary experiment, as outlined in Section 2, and the results are provided in ref. [25].

Figs. 7–10 show the experimentally measured temperature changes over time for the four operation modes for a constant input thermal load and orientation. The temperatures detected by the thermocouples installed on the outer wall of the bypass tube (T_{BL1} and T_{BL2} in Fig. 5) for predicting the bypass flow are indicated in red. Fig. 7 shows the temperature changes at designated horizontal locations over time for NOM (Fig. 7(a)), BOM I (Fig. 7(b)), BOM II (Fig. 7(c)), and BOM III(Fig. 7(d)) for an input thermal load of 200 W. For the NOM (Fig. 7(a)), all surface temperatures of the heat pipe reached a steady-state condition after 105 min. The maximum surface temperature was recorded by a thermocouple installed at the start of the evaporator ($T_{eva.1}$); this temperature was raised to 104.9 °C when the steady state was achieved. In Figs. 7(b)–7(d), the bypass starting time (BST), which is the elapsed time for the bypassed liquid to reach the evaporator, decreased as the number of activated bypass ports increased. The BST was defined as the time at which the temperature measured at the start of the evaporator (T_{BL1}), which continuously increases owing to the temperature increase of the evaporator, suddenly begins to decrease owing to cooling from the bypassed liquid. The BST for BOM I, II, and III were 15.9, 14.5, and 11.5 min, respectively. For the BOMs, a temperature overshoot was observed at the outer surface of the evaporator during startup because the time taken for the bypassed liquid to reach the evaporator was delayed.

As shown in Fig. 7(b)–(c), the overshoot for the outer wall temperature of the evaporator was measured in $T_{eva.1}$ and $T_{eva.2}$. As shown in these figures, the temperature overshoot starts to decrease when the BST is measured and completely disappears when a steady state is reached. During the overshoot, the evaporator wall temperatures were higher for $T_{eva.1}$ than for $T_{eva.2}$, similar to the trend of NOM; however, after reaching BST, $T_{eva.2}$ was higher than $T_{eva.1}$. The evaporator wall temperatures could rise significantly close to the NOM level because the BOM was not achieved before reaching the BST, and the heat pipe operation was the same as that of the NOM in Fig. 7(a). However, when the heat-pipe operation reaches the BST, the wall temperatures are reduced by supplying condensed liquid to the start of the evaporator through the bypass flow. Therefore, a methodology for designing the bypass line to minimize BST is required to mitigate the temperature

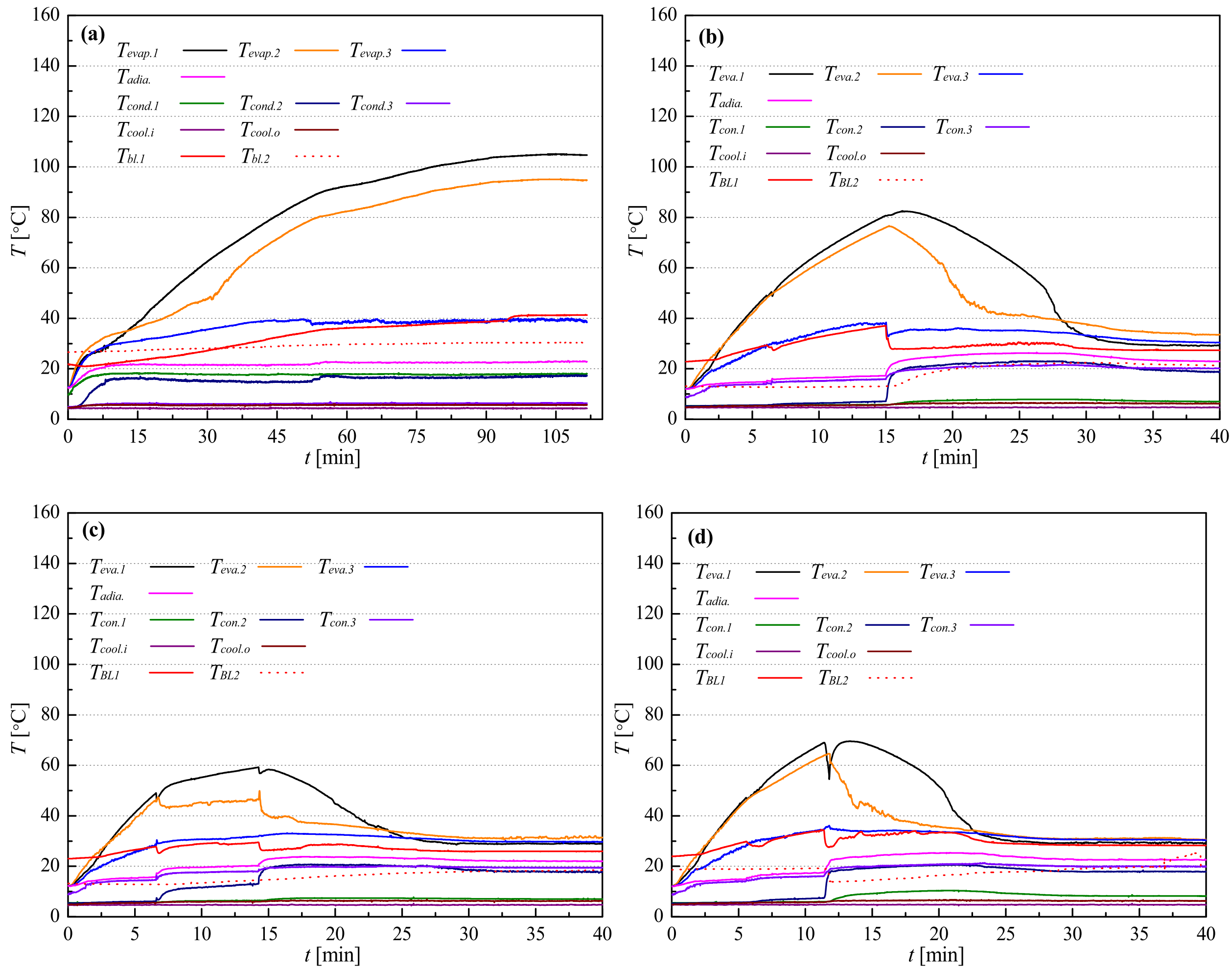

Fig. 7. Temperature history for $\varphi = 0^\circ$ (horizontal) with a Q_{in} of 200 W for all four operating modes: (a) NOM, (b) BOM I, (c) BOM II, and (d) BOM III.

overshoot. For the bypass line activated modes (BOM I, BOM II, and BOM III), relatively low temperatures were measured at the start of the evaporator because the liquid was bypassed from the condenser to the start ($T_{eva.1}$). In contrast to NOM, the maximum temperature of the outer surface of the evaporator was recorded by a thermocouple installed at the center of the evaporator wall ($T_{eva.2}$). This maximum temperature decreased as the number of activated bypass ports increased, owing to the increase in the bypass flow rate. The maximum temperatures of the outer wall of the evaporator were 33.8 °C, 31.5 °C, and 30.5 °C for BOM I, II, and III, respectively; the lowest value (BOM III) was 74.4 °C lower than the corresponding value recorded for the NOM.

Fig. 8 shows the temperature changes at major positions of the heat pipe over time for the NOM (Fig. 8(a)), BOM I (Fig. 8(b)), BOM II (Fig. 8(c)), and BOM III (Fig. 8(d)) for $\varphi = 20^\circ$ and $Q_{in} = 600$ W. For the NOM (Fig. 8(a)), the maximum temperature was measured on the external surface at the start of the evaporator, as in the horizontal position; this maximum temperature was 79.8 °C in the steady state. As shown in Figs. 8(b)– 8(d), the maximum temperature of the external surface of the evaporator decreased as the number of activated bypass ports increased, owing to the increase in the bypass mass flow rate. Under NOM, BOM I, BOM II, and BOM III, the maximum temperatures were 80.3 °C, 75.8 °C, 73.8 °C, and 70.7 °C, respectively; the maximum temperature with the bypass modes was up to 9.6 °C lower compared with that without (NOM). In addition, overheating of the external surface of the evaporator for NOM was not observed with the bypass modes because gravity helped the bypassed liquid rapidly reach the evaporator. Figs. 8(a)– 8(d) show that T_{BL1} decreased when the bypassed liquid reached the evaporator. For the BOM, the average temperature of the external surface of the evaporator ($\overline{T}_{eva.}$) generally decreased, except in the case of BOM I. While $\overline{T}_{eva.}$ was 74.3 °C for the NOM, $\overline{T}_{eva.}$ was 72.7 °C and 63.6 °C for BOM II and BOM III, respectively; it decreased by up to 10.7 °C. For BOM I (Fig. 8(b)) and BOM III (Fig. 8(d)), the temperatures at the closing of the condenser ($T_{cond.3}$) were significantly higher than that of NOM; $T_{cond.3}$ was 27 °C for the NOM but increased to 62 °C for BOM I apparently, because a higher steam flow rate from the evaporator reaches the end of the condenser for some BOM operations.

Fig. 9 shows the temperature changes at major positions of the heat pipe over time with $\varphi = 40^\circ$ and $Q_{in} = 700$ W. Under the NOM, the maximum temperature of the outer wall of the evaporator increased to 103.4 °C in the steady state, and $\overline{T}_{evap.}$ was 90 °C. Figs. 9(a)– 9(d) present that the maximum wall temperatures of the evaporator were lower for the BOM than for the NOM; this maximum temperature was 85 °C, 83.5 °C, and 79.2 °C for BOM I, BOM II, and BOM III, respectively, which is up to 24.2 °C lower compared to that for the NOM. The average wall temperatures of the evaporator were 80.9 °C, 79.8 °C, and 74.2 °C for BOM I, BOM II, and BOM III, which is up to 15.8 °C lower compared to that for the NOM. Fig. 9 depicts that the temperature of the outer wall of the evaporator generally decreased as the number of activated bypass ports increased for a Q_{in} of 700 W, indicating an improvement in heat transfer performance in the steady state. As the inclination angle increased, a liquid pool was produced at the start of the evaporator and acted as thermal resistance. Accordingly, the temperature measured at the start of the evaporator ($T_{evap.1}$) was the highest under all operation modes.

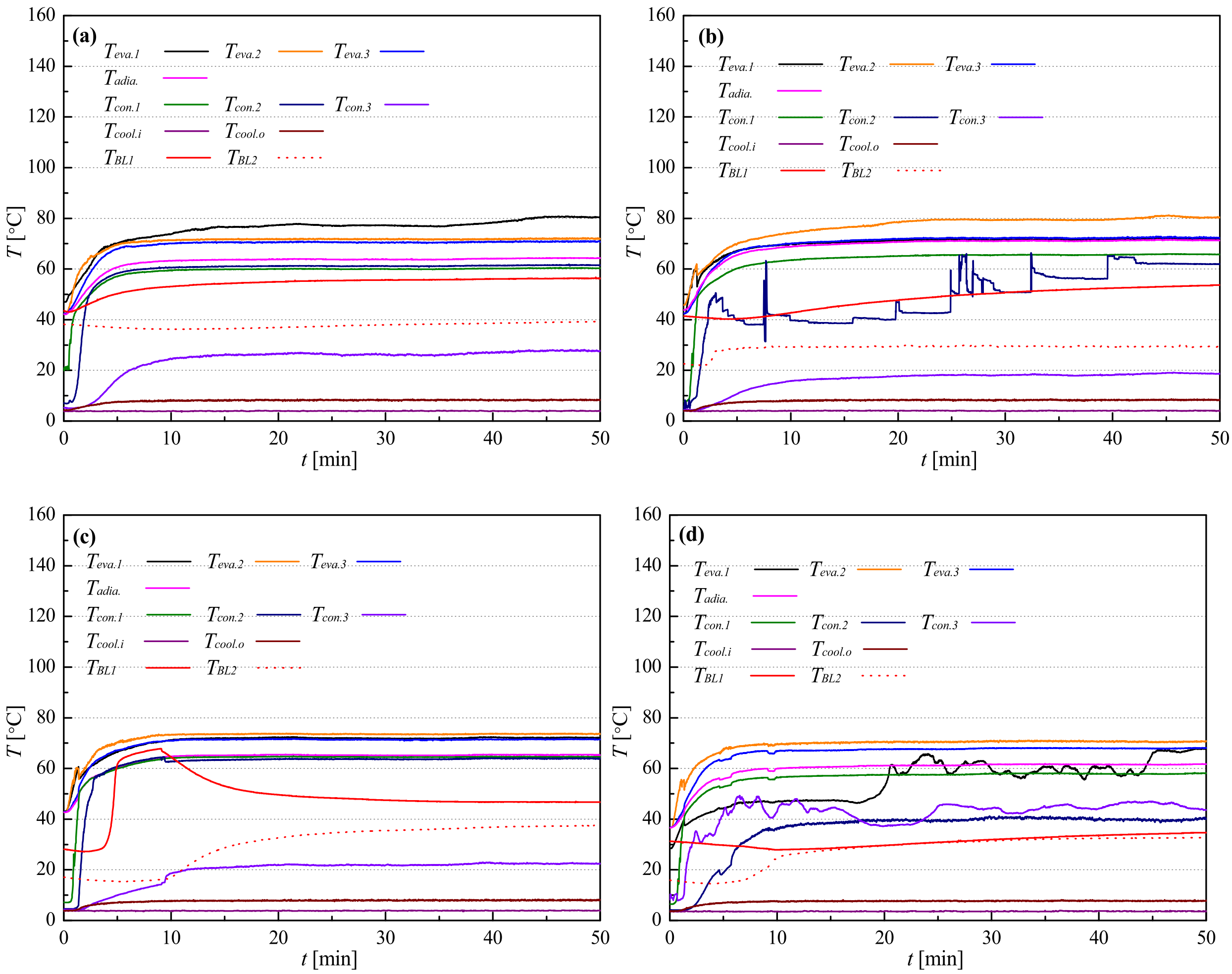

Fig. 8. Temperature history for $\varphi = 20^{\circ}$ with a Q_{in} of 600 W for all four operating modes: (a) NOM, (b) BOM I, (c) BOM II, and (d) BOM III.

Fig. 10 shows the temperature history for each operation mode with $\varphi = 50^{\circ}$ and $Q_{in} = 700$ W. Under the NOM, the maximum and average temperatures of the external surface of the evaporator were 101.7 °C and 91 °C, respectively. Figs. 10(a)– 10(d) show that the maximum and average temperatures of the external surface of the evaporator decreased under the influence of bypass flow. Under BOM I, BOM II, and BOM III, the maximum temperatures of the external surface of the evaporator were 79.1 °C, 77.5 °C, and 77.1 °C, respectively; the values for BOM II and BOM III were very similar, and all values were up to 24.6 °C smaller than that for the NOM. $\overline{T}_{evap.}$ was 79.1 °C, 77.5 °C, and 77.2 °C for BOM I, BOM II, and BOM III, respectively, which were up to 13.8 °C lower than that for the NOM. For the BOMs, the external surface temperature of the bypass decreased at the startup time owing to bypass flow (Fig. 10). However, over time, the wall temperature of the bypass line tended to increase as the outer wall of the condenser increased.

As shown in Figs. 7–10, the maximum and average temperatures of the external surface of the evaporator generally decreased as the number of activated bypass ports increased owing to the increase in the liquid-bypass mass flow rate. The liquid that was subcooled and condensed in the condenser was directly bypassed to the start of the evaporator without going through the heat pipe. Therefore, increasing the bypassing mass flow rate of the working fluid in the design of a bypass tube is key to improving the thermal performance under the normal operation of the heat pipe.

Additionally, as shown in Figs. 8(b), 8(d), 9(a), and 10(b), the temperature oscillations on the walls of the evaporator and condenser were measured. The temperature oscillation on the wall of the heat pipe under capillary flow with boiling or condensation is mainly caused by bubble formation [26,27]. Heat transfer may be suppressed by the bubbles generated under nucleate boiling; the temperature may increase, and the wall temperature may decrease because of the activation of heat transfer as the bubbles disappear. The temperature oscillation of the heat-pipe wall can be measured during nucleate boiling. Temperature oscillations can often be measured as a liquid pool produced at the start of the evaporator under a gravity-assisted orientation. In addition, temperature oscillations can be measured for condenser walls with bubbly flows.

Fig. 11 shows the R_{th} for different Q_{in} for all four operation modes with $\varphi = 0^{\circ}$ (horizontal). NOM yielded the highest thermal resistance, whereas BOM III yielded the lowest. For the NOM with a Q_{in} of 200 W, a sharp increase in R_{th} occurs; this is close to the thermal load value that causes dry-out. For a Q_{in} of 250 W, steady-state heat transfer was impossible owing to dry-out. However, a Q_{in} of up to 350 W could be stably supplied for BOM III. The R_{th} sequentially lowered as the number of activated bypass ports increased. For a Q_{in} of 150 W, the thermal resistance under BOM III was 25.5% lower than that for the NOM. For a Q_{in} of 50 W, the R_{th} under BOM I was only 0.8% lower than that for the NOM; this is an insignificant difference.

Fig. 12 shows the R_{th} for different Q_{in} for all four operation modes with $\varphi = 20^{\circ}$. The BOMs generally yielded a lower thermal resistance than the NOM, except for Q_{in} of 100 and 200 W. In this case, which corresponds to a relatively low thermal range, normal liquid-bypass flow may not be produced owing to insufficient vapor arrival in the condenser. Because sufficient liquid-bypass flow is not generated under a low thermal load, the heated liquid leaks into the bypass tube located at the start of the evaporator, and the thermal resistance may increase.

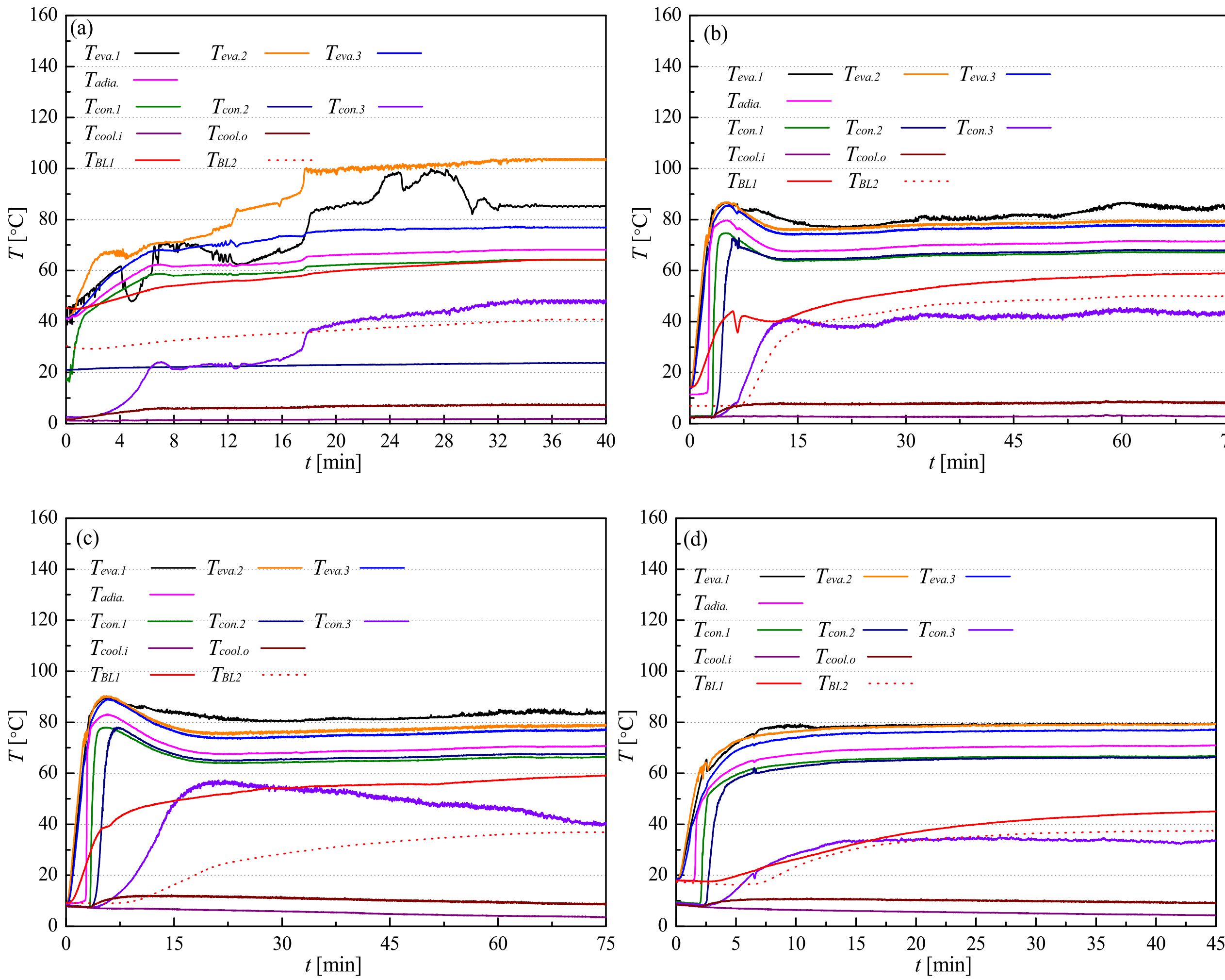

Fig. 9. Temperature history for $\varphi = 40^\circ$ with a Q_{in} of 700 W for all four operating modes: (a) NOM, (b) BOM I, (c) BOM II, and (d) BOM III.

Under an input thermal load of 100 W, the difference in thermal resistance between NOM and BOMs (BOM I and BOM III) was less than 1%. However, the thermal resistance of BOM II increased by approximately 2% compared to that of NOM. Under an input thermal load of 200 W, the thermal resistance of the BOMs was higher than that of NOM, and in the case of BOM II, it increased by up to 5.3% compared to NOM. Under an input thermal load of 200 W, the thermal resistance of BOMs (BOM I and BOM III) was higher than that of NOM overall but increased by up to 5.3% compared to that of NOM under BOM II. Because the bypassed liquid is not sufficient under a low thermal load, leakage in the bypass tube of the liquid heated in the evaporator was unavoidable; thus, the increase in thermal resistance was generally evaluated to be less than 5%. In the thermal load range of 200 W or more, the thermal resistance of the heat pipe was significantly lowered by liquid-bypass application. The lowest thermal resistance was measured for BOM III. For a Q_{in} of 600 W, the R_{th} was 0.0488 °C/W and 0.01983 °C/W for the NOM and BOM III, respectively; this is a reduction of up to 59.4%. For a Q_{in} of 100 W, the thermal resistance under BOM I was slightly higher than that for the NOM. At a low Q_{in}, the liquid bypass from the start of the condenser had an unfavorable effect on thermal performance apparently because the average wall temperature of the evaporator increased owing to the bypass of the liquid that had not been sufficiently cooled.

Fig. 13 shows the R_{th} for different Q_{in} for all four operation modes with $\varphi = 50^\circ$. Except for Q_{in} of 100 W, low thermal resistance was generally obtained under all bypass operation modes. However, for a Q_{in} of 100 W, the R_{th} for BOM I was 3.2% greater than that for the NOM. For a Q_{in} of 700 W, the R_{th} for BOM III was 51.6% lower than that for the NOM. At a Q_{in} of 500 W, the R_{th} levels were equivalent for the NOM and BOM I. Unusually, BOM I exhibited the lowest thermal resistance for a R_{th} of 200 W because the mass flow rate bypassed from the condenser had extremely complex and different tendencies depending on the Q_{in}. As the Q_{in} increased, the thermal resistance became lowest for BOM III because for BOM III, the highest mass flow rate was bypassed as all bypass ports were activated. Consequently the steady state was reached stably for BOM III for a Q_{in} of 800 W, even though this was impossible with the NOM owing to dry-out.

Fig. 14 compares the R_{th} of the NOM and BOM III cases for different orientations of the heat pipe for a Q_{in} of 500 W. Except for a few unusual cases, the thermal resistance was the lowest for BOM III. At $\varphi = 10^\circ$, 20°, 30°, 40°, and 50°, the thermal resistances under BOM III were 16.2%, 11.9%, 18.4%, and 15.8% lower than those for the NOM, respectively.

Figs. 15 and 16 show the maximum wall temperatures of the evaporator for different input thermal loads, with all four operation modes and with $\varphi = 0^\circ$ and 40°. At $\varphi = 0^\circ$, the maximum temperature for the BOMs was generally lowered with increased bypass ports activated. However, for a Q_{in} of 100 W, the maximum temperature was lowest for BOM I, but the temperature difference between all operation modes was less than 2.5 °C. For a Q_{in} of 200 W, the difference in maximum temperature between the NOM and BOM III cases was 76.6 °C. At $\varphi = 40^\circ$, the maximum temperature was generally lower for the BOMs than for the NOM. For a Q_{in} of 700 W, the maximum temperature was lower for the BOMs, and the temperature differences between the NOM and BOM I, BOM II, and BOM III were 18.7 °C, 20.2 °C, and 24.5 °C, respectively.

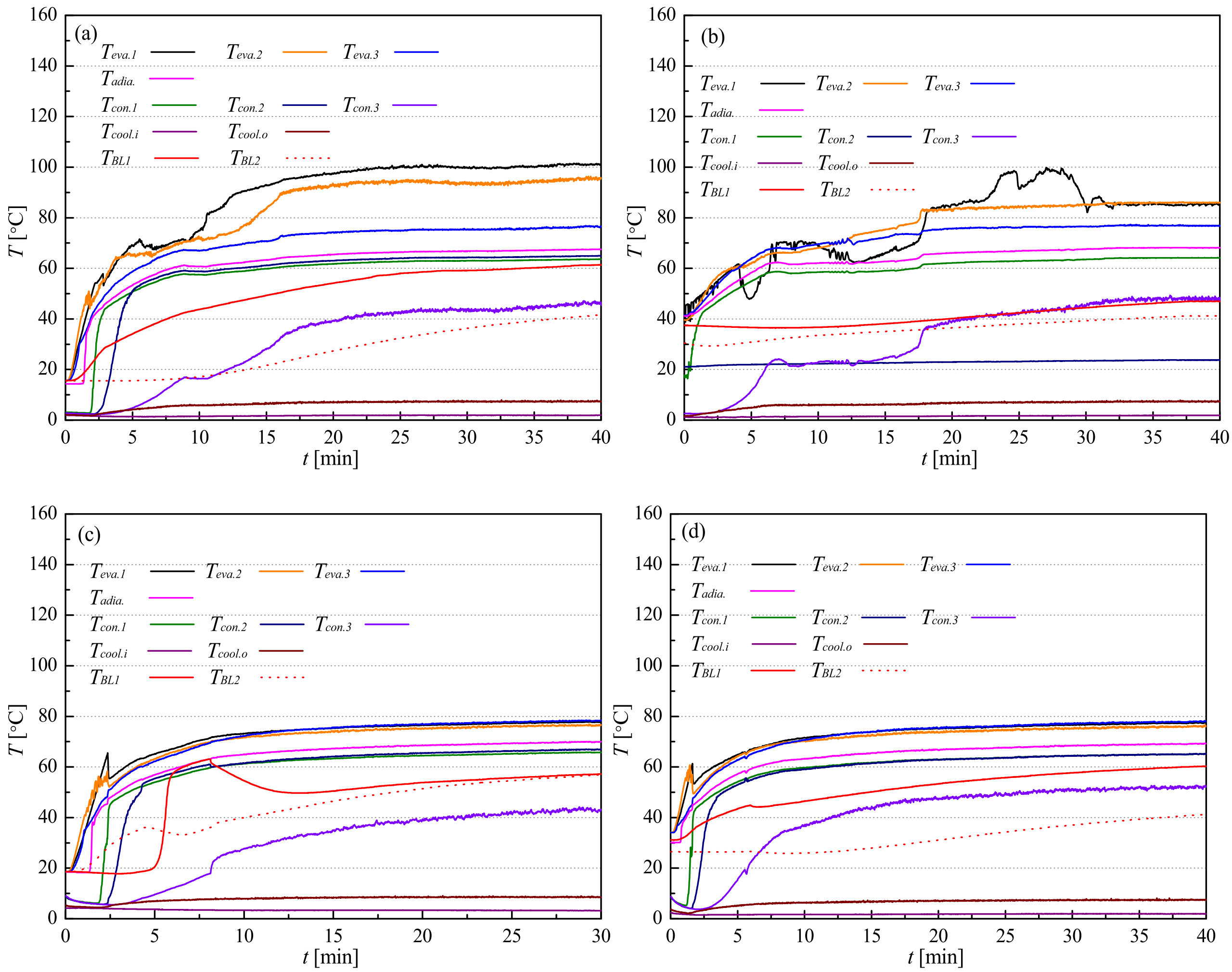

Fig. 10. Temperature history for $\varphi = 50^\circ$ with a Q_{in} of 700 W for all four operating modes: (a) NOM, (b) BOM I, (c) BOM II, and (d) BOM III.

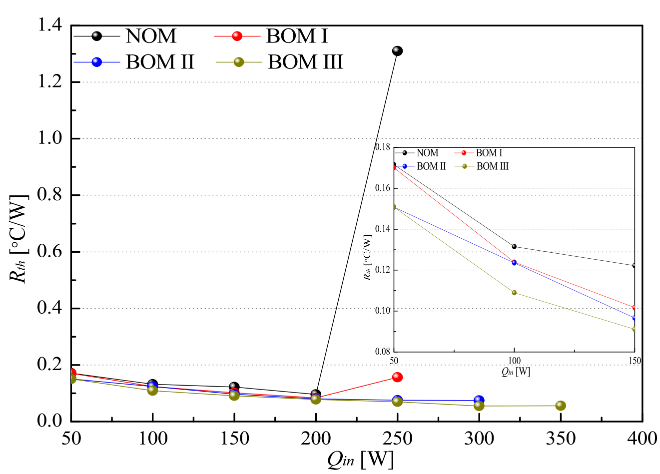

Fig. 11. Comparison of R_{th} for different Q_{in} for all four operating modes with $\varphi = 0^\circ$.

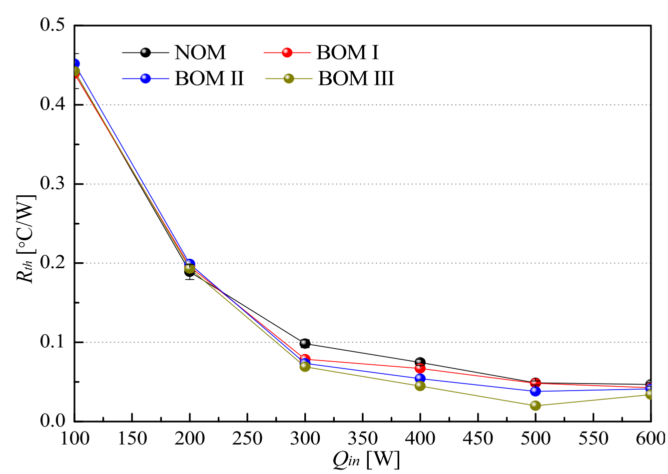

Fig. 12. Comparison of R_{th} for different Q_{in} for all four operating modes with $\varphi = 20^\circ$.

4. Conclusions

In this study, experiments were performed to investigate the influence of liquid-bypass mass flow rate on the thermal performance of a heat pipe. The main experimental variables were the tilt angle of the heat pipe, operation mode, and input thermal load. Bypass ports were installed at the start, middle, and end of the condenser to consider the effect of the liquid-bypass mass flow rate on the performance of the heat pipe. An ON/OFF valve was attached to each bypass port to regulate bypass flow. Four operation modes were defined: the bypass mass flow rate increased as the bypass ports were sequentially activated from the start of the condenser. The tilt angle of the heat pipe increased from

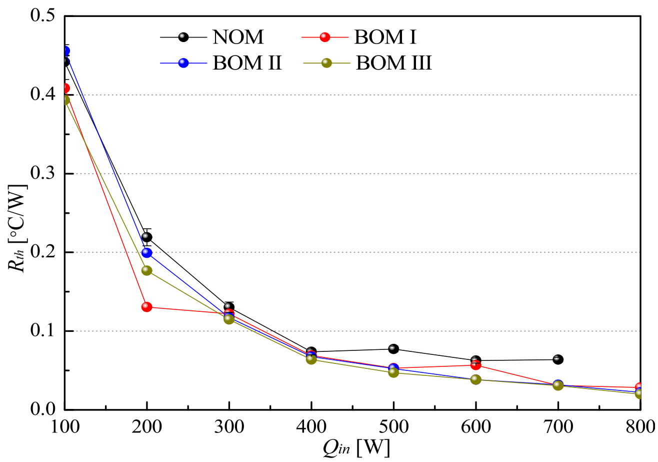

Fig. 13. Comparison of R_{th} for different Q_{in} for all four operating modes with $\varphi = 50°$.

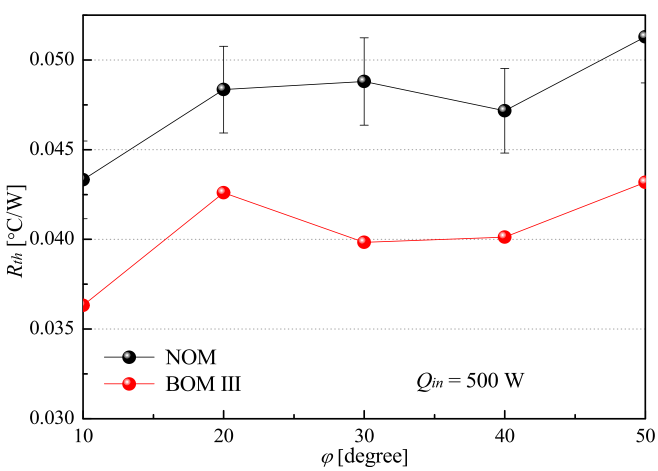

Fig. 14. Comparison of R_{th} for different φ for NOM and BOM III with Q_{in} = 500 W.

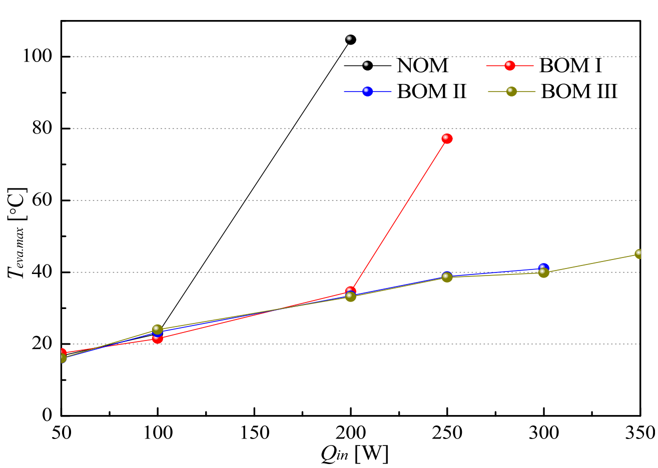

Fig. 15. Comparison of maximum wall temperature for different Q_{in} for all four operating modes with $\varphi = 0°$.

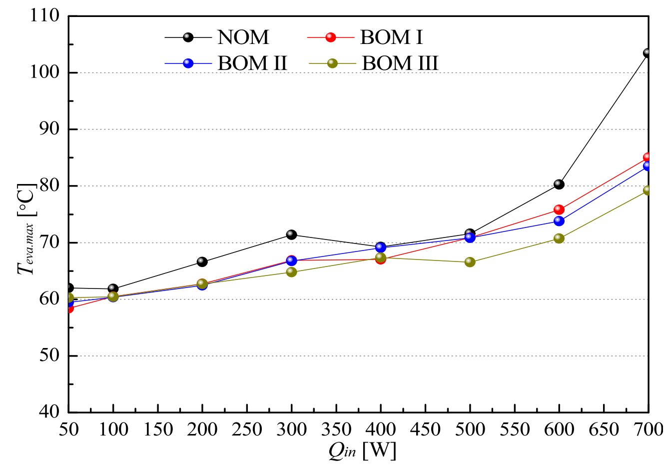

Fig. 16. Comparison of maximum wall temperature for different Q_{in} for all four operating modes with $\varphi = 40°$.

0° (horizontal position) to 50°. Based on the results, the following conclusions were drawn:

(1) As the number of activated liquid ports installed in the condenser increased, the maximum temperature of the external surface of the evaporator decreased owing to the increase in the bypass mass flow rate. For example, for a horizontal orientation, the wall temperature of the heat pipe decreased by up to 74.4 °C when all the installed bypass valves were opened.
(2) In the horizontal position, a temperature overshoot was measured at the external surface of the evaporator during startup because of the delay in bypass completion. The time required for startup decreased as the number of activated bypass ports increased.
(3) Under the bypass flow, the thermal resistance decreased as the average wall temperature of the evaporator decreased. The lowest thermal resistance was obtained when all the bypass valves were opened. At a heat-pipe tilt angle of 20°, the heat-transfer performance decreased by up to 59.4% (Q_{in} = 600 W) when all the bypass valves were opened.
(4) Under the application of a liquid bypass, the flow resistance to the inner space of the heat pipe was reduced, thereby improving the heat-transfer performance by accelerating the working fluid.

These results confirm that the transient and steady-state heat-transfer performance of a heat pipe can be enhanced by adding a bypass line, owing to a reduction in the flow resistance inside the heat pipe. Although loop-type heat pipes follow the same principle, bypass lines are structurally simpler and easier to produce. The design of the bypass flow path from the condenser must be carefully considered to bypass as much liquid as possible to maximize the heat-transfer performance of a heat pipe under a liquid-bypass flow.

Declaration of Competing Interest

None.

Data availability

No data was used for the research described in the article.

Acknowledgment

This work was supported by a National Research Foundation (NRF) grant funded by the Ministry of Science (Nos. NRF-2022R1F1A1066459 and NRF-2022R1A2C1009690). he university innovation support project supported this research through the National Research Foundation of Korea, funded by the Ministry of Education.

References

[1] Z. Gaugler, Heat pipe design and technology: modern applications for practical thermal management, Springer, 2016, pp. 1–50.

[2] Z. Kang, Y. Hong, S. Jiang, J. Fan, Composite filament with super high effective thermal conductivity, Mater. Today Phys. 34 (2023) 101067.

[3] D.M. Weragoda, G. Tian, A. Burkitbayev, K.H. Lo, T. Zhang, A comprehensive review on heat pipe based battery thermal management systems, Appl. Therm. Eng. 18 (2023) 120070.

[4] Z. Li, H. Zhang, Z. Huang, D. Zhang, H. Wang, Characteristics and optimization of heat pipe radiator for space nuclear propulsion spacecraft, Prog. Nucl. Energy 150 (2022) 104307.

[5] V.K. Patel, An efficient optimization and comparative analysis of ammonia and methanol heat pipe for satellite application, Energy Convers. Manag. 165 (2018) 382–395.

[6] Y. Li, N. Li, B. Shao, D. Dong, Z. Jiang, Theoretical and experimental investigations on the supercritical startup of a cryogenic axially Ω-shaped grooved heat pipe, Appl. Therm. Eng. 222 (2023) 119951.

[7] J. Zhao, Y. Ji, D.Z. Yuan, Y.X. Guo, S.W. Zhou, Structural effect of internal composite wick on the anti-gravity heat transfer performance of a concentric annular high-temperature heat pipe, Int. Commun. Heat Mass Transf. 139 (2022) 106404.

[8] Z. Zhao, G. Peng, Y. Zhang, D. Zhang, Heat transfer performance of flat micro-heat pipe with sintered multi-size copper powder wick, Case Stud. Therm. Eng. 42 (2023) 102720.

[9] S.C. Wong, Y.C. Lin, J.H. Liou, Visualization and evaporator resistance measurement in heat pipes charged with water, methanol or acetone, Int. J. Therm. Sci. 52 (2012) 154–160.

[10] W. Zhou, Y. Li, Z. Chen, L. Deng, B. Li, Experimental study on the heat transfer performance of ultra-thin flattened heat pipe with hybrid spiral woven mesh wick structure, Appl. Therm. Eng. 170 (2020) 115009.

[11] G. Huang, W. Liu, Y. Luo, Y. Li, H. Chen, Fabrication and capillary performance of a novel composite wick for ultra-thin heat pipes, Int. J. Heat Mass Transf. 176 (2021) 121467.

[12] S. Huang, Z. Wan, X. Zhang, X. Yang, Y. Tang, Evaluation of capillary performance of a stainless steel fiber-power composite wick for stainless steel heat pipe, Appl. Therm. Eng. 148 (2019) 1224–1232.

[13] S.C. Wong, M.S. Deng, M.C. Liu, Characterization of composite mesh-groove wick and its performance in a visualizable flat-plate heat pipe, Int. J. Heat Mass Transf. 184 (2022) 122259.

[14] S.M. Henein, A.A. Abdel-Rehim, The performance response of a heat pipe evacuated tube solar collector using MgO/MWCNT hybrid nanofluid as a working fluid, Case Stud. Therm. Eng. 33 (2022) 101957.

[15] M. Zhang, Z. Liu, G. Ma, S. Cheng, The experimental study on flat plate heat pipe of magnetic working fluid, Exp. Thermal Fluid Sci. 33 (2009) 1100–1105.

[16] V. Ayel, M. Solbodeniuk, R. Bertossi, A. Karmakar, F. Martineau, C. Romestant, Y. Bertin, S. Khandekar, Thermal performances of a flat-plate pulsating heat pipe tested with water, aqueous mixtures and surfactants, Int. J. Therm. Sci. 178 (2022) 107599.

[17] Y.F. Maydanik, Loop heat pipes, Appl. Therm. Eng. 25 (2005) 635–657.

[18] Y. Wu, J. Cheng, H. Zhu, H. Xue, Q. Lu, Y. Li, W. Li, H. Tao, Experimental study on heat transfer characteristics of separated heat pipe with compact structure for spent fuel pool, Ann. Nucl. Energy 181 (2023) 109580.

[19] Z. Kang, D. Shou, J. Fan, Numerical study of single-loop pulsating heat pipe with porous wicking layer, Int. J. Therm. Sci. 179 (2022) 107614.

[20] Z. Kang, D. Shou, J. Fan, Numerical study of a novel single-loop pulsating heat pipe with separating walls within the flow channel, Appl. Therm. Eng. 196 (2021) 117246.

[21] Z. Kang, S. Jiang, Y. Hong, J. Fan, Squid-like soft heat pipe for multiple heat transport, Droplet 1 (2022) 182–191.

[22] Z. Kang, J. Fan, Heat-pipe-based tunable multimode horizontal thermal rectifier, Energy Rep. 8 (2022) 4274–4281.

[23] E.G. Jung, J.H. Boo, Enhancement of the maximum heat transfer rate of the heat pipe through the bypass line, Appl. Therm. Eng. 198 (2021) 117461.

[24] Y.M. Baek, E.G. Jung, Experimental study on start-up and steady-state heat transfer performance of heat pipe with liquid bypass line for accelerating working fluid, Case Stud. Therm. Eng. 29 (2022) 101708.

[25] C.H. Kwon, G.C. Jin, J.H. Kim, B.G. Im, J.H. Jeong, E.G. Jung, Influence of condenser bypass port area on maximum thermal load of heat pipe, Int. Commun. Heat Mass Transf. 148 (2023) 107006.

[26] X. Ji, J. Xu, H. Li, G. Huang, Switchable heat transfer mechanisms of nucleation and convection by wettability match of evaporator and condenser for heat pipes: nanostructured surface effect, Nano Energy 38 (2017) 313–325.

[27] I. Muraoka, F.M. Ramos, V.V. Vlassov, Analysis of the operational characteristics and limits of a loop heat pipe with porous element in the condenser, Int. J. Heat Mass Transf. 44 (2001) 287–297.

[28] J.P. Holman, Experimental Methods for Engineers, McGraw-Hill, 1996.